Since the reduction currents were increased nearly by a factor of two in the presence of SDS (Figure 1d), the yield of $Ru(bpy)_3^+$ may be assumed to be doubled, followed by doubling the yield of SO_4^-. Therefore ϕ_{ex} from Eq. (3) may be assumed to gain four fold increase at most in the SDS micellar environment.

Now, taking into account the 20% increase in ϕ_f, one may expect ϕ_{cl} to be increased at most by a factor of 4.8 from Eq. (4). However, as shown in Figure 5 experimental data suggest that the relative ECL intensity exceeds the expected increase above 5.0×10^{-3} M SDS. That is, the increases in ϕ_{ex} and ϕ_f cannot account for the large increase in ECL intensity *vs.* [SDS] beyond 5.0×10^{-3} M SDS. The cause of the additional increase in ϕ_{cl} is speculated due to the stabilization of the reduction intermediate $Ru(bpy)_3^+$ and/or SO_4^-. The explanation may be supported by a recent report, where the electrochemically produced anion radical of nitrobenzen was greatly stabilized for a relatively strong interaction between the radical and the SDS micellar environment.[5] In addition $Ru(bpy)_3^+$ can associate more strongly with SDS micellar core than $Ru(bpy)_3^{2+}$ by hydrophobic interaction.[7] Furthermore, the duration time, defined as the time required for ECL intensity to decay to zero, was lengthened in the presence of SDS micelles as can be seen from Figure 5 and Table 2, which possibly support the stabilization of the reaction intermediate.

Lastly, it was considered to be worth mentioning the possibility of adsorption of SDS on Pt electrode. Bard *et al.*[1b] have reported that the oxidation potential of $Ru(bpy)_3^{2+}$ in the presence of liver tissue shifts to a higher potential due to possible adsorption of the biological compound, thus changing the surface properties of the electrode. The shift of oxidation potential occurs also $Os(bpy)_3^{2+}$ interacts with SDS micelles by a strong hydrophobic interaction.[6]

In the present study, however, no such potential shift was observed for the reduction of $Ru(bpy)_3^{2+}$ in the presence of SDS at Pt electrode (Figure 1d). Thus it appears unlikely to assume that SDS micelles were adsorbed on Pt electrode. For negatively charged SDS micelles were presmably repelled from the cathode. Furthermore, since hydrogen was being evolved at Pt electrode over the pontential region negative of −1.4 V, SDS was apparently prevented from adsorbing to the electrode surface.

Therefore the ECL enhancement in this study appears not to be attributable to the adsorption of SDS on Pt electrode. Rather, it could be due to the solubilization of reactants and possible stabilization of ECL intermediates in the SDS micellar environment.

Acknowledgement. We are grateful for the financial support for this work from the Korea Science and Engineering Foundaiton.

References

1. (a) I. Rubinstein, C. R. Martin and A. J. Bard, *Anal. Chem.*, **55**, 1580 (1983); (b) D. Ege, W.G. Becker and A.J. Bard, *ibid.*, **56**, 2413 (1984).
2. H .S. White and A. J. Bard, *J. Am. Chem. Soc.*, **104**, 6891 (1982).
3. W. L. Wallace and A. J. Bard, *J. Phys. Chem.*, **83**, 1350 (1979).
4. G. Meyer, L. Nadjo and J. M. Saveant, *J. Electroanal. Chem.*, **119**, 417 (1981).
5. H. N. Blount, G. L. McIntire, D. M. Chiappardi, and R. L. Casselberry, *J. Phys. Chem.*, **86**, 2632 (1982).
6. J. Oyang and A. J. Bard, *Bull. Chem. Soc. Jpn.*, **61**, 17 (1988).
7. (a) I. Rubinstein and A. J. Bard, *J. Am. Chem. Soc.*, **102**, 6641 (1980); (b) A. E. Kaifer and A. J. Bard, *J. Phys. Chem.*, **89**, 4876 (1985).
8. L. L. Klopf and T. A. Nieman, *Anal. Chem.*, **56**, 1539 (1984).
9. T. E. Riehl, C. L. Malenhorn and W. L. Hinze, *Analyst*, **111**, 931 (1986).

A Study of Phase Transition of Lipids and Lipid Mixtures by Differential Scanning Calorimetry

Nam Hong Kim, Sung Bae Roh, and Won Woo Park*

College of Pharmacy, Pusan National University, Pusan 609-390
**Department of Industrial Chemistry, Pusan Junior College, Pusan 616-092*
Received May 10, 1990

The simple binary mixtures of pure phospholipids such as DPPC:DSPC and DPPC:DPPA were investigated with differential scanning calorimeter. The thermotropic properties of DPPC and DSPC mixtures did not deviate much from the ideal curves that was obtained on varying either the temperature or the relative proportions of phospholipids. This means that the two phospholipids are completely miscible in the liquid and solid phase. But the thermotropic properties of DPPC and DPPA mixture deviated much from the ideal phase diagram. It resulted from the repulsion between the head groups of acidic phospholipids. Heat capacity suggested by Harden McConell was calculated. The larger C_p was, the sharper the endothermic peak became.

Introduction

The phase transition properties of lipid mixtures have been studied extensively[1-4]. Ideal mixing has been observed with the lipids of the head group and differing only slightly in alkyl chain length. The mixing properties of lipid depend on the factors that determine packing of the chains as well as the interaction between the polar groups. Mixing in the gel phase is particularly constrained because of a close-packing organization

Biological membranes are a complex mixture of phospholipid species which vary with respect to both their lipid headgroup and to their associated acyl chains. As a result they do not exhibit a single well-defined lipid phase transition where all of the lipid progresses from a solid to a fluid state at a well defined temperature. A lipid phase separation in a biological membrane results in the coexsitence, over a particular temprature range, of two or more distint types of lipid phase with different chemical compositions[4]. Most often the primary distinguishing feature between these two lipid phases is that one consists of solid-solid phase lipid and the other fluid-phase lipid. However, fluid-fluid and solid-solid immiscibility has been noted.

It is worth examing simple binary mixtures of pure phospholipids in order to appreciate some of the phenomena that are likely to be encountered in the much more complex situation found with biological membranes.

Experimental

Materials. Dipalmitoyl L-α-phosphatidylcholine (DPPC), distearoyl L-α-phosphatidylcholine (DSPC) and dipalmitoyl L-α-phosphatidic acid (DPPA) and stearic acid were purchased from Sigma Chemical Company (U.S.A.) and used as received. Water was deionized distilled water. Other reagents were all reagent grades. The buffer used for all measurements was 0.1 M KCl/0.01 M Tris/0.1 mM EDTA adjusted to pH 7.4.

Preparation of Multilamellar Liposomes for Differential Scanning Calorimetry. The chloroform solution containing purified from a newly opened ampoule was transferred to a glass tube which had been flushed with nitrogen. The chloroform was then evaporated under vacuum[5-7]. The dried lipids were suspended in buffer adjusted to pH 7.4 above the phase transition temperature with a vortex mixer for 10 min and multilamellar liposomes were obtained.

Differential Scanning Calorimetry (DSC). The phase transition temperature of the phospholipid dispersions was determined with a Shimadzu differential scanning calorimeter, SC30, accordingly to the usual methods[8,9].

Each sample was scanned between 30 °C and 80 °C at a rate of 2 °C/min and a range of 5 mJ/sec. Transition enthalpy was determined from the ratio of the area under endothermic curve of phospholipid sample to that of stearic acid as calibrant (T_m = 69.5 °C, ΔH = 16.4 Kcal/mole).

Calculation for C_p (heat capacity) of Liposomal Lipid Bilayers.

Phase Diagram of Phase Transition of Mixed Phospholipids. If in the mixture of two lipids A and B, the phase equilibrium constant of the lipid A at temperature T is K_A^1 and the phase equilibrium constant at the main transition temperature T_A is K_A^2, the following equation can be obtained[10,11].

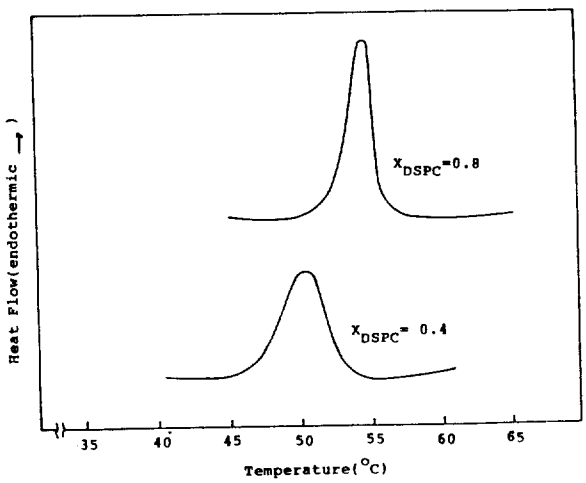

Figure 1. Calorimetric transition curves for mixture of DPPC and DSPC.

$$\ln K_A^2/K_A^1 = \Delta H_A^0/R\,(1/T - 1/T_A) \tag{1}$$

The same relation for the lipid B holds.

$$\ln K_B^2/K_B^1 = \Delta H_B^0/R\,(1/T - 1/T_B) \tag{2}$$

If α and β are defined as follows,

$$\alpha = K_A^2/K_A^1 = \exp\,(\Delta H_A^0/R\,(1/T - 1/T_A)) \tag{3}$$

$$\beta = K_B^2/K_B^1 = \exp\,(\Delta H_B^0/R\,(1/T - 1T_B)) \tag{4}$$

the ideal phase diagrams of the mixture can be computed by means of the following relations.

$$X_B^1 = (1-\alpha)/(\beta-\alpha)\ :\ X_B^S = \beta X_B^1 \tag{5}$$

Here, X_B^S and X_B^1 are the mole fractions of lipid in crystalline state and liquid-crystalline state at a specific temperature.

Calculation for C_p (heat capacity) of Liposomal Lipid Bilayers. It has been pointed out by Harden McConnell that the phase diagram gives all the information needed to calculate theoretical transition curves, if one neglects the heat effects associated with unmixing the solid components and mixing the liquid components during the transition. It is evidence that, for one mole of total lipid[11],

$$dH/dT = C_p = \Delta H_A\, d\,(f^{(S)} X_A^{(S)})/dT + \Delta H_B d\,(f^{(S)} X_B^{(S)})/dT \tag{6}$$

where H and C_p are excess quantities, and the fraction, $f^{(S)} = (X_B - X_B^1)/(X_B^S - X_B^1)$.

Differentiation, as indicated in eq (11), leads to the result,

$$C_p = \frac{X_A^1 \Delta H_A + X_B^1 \Delta H_B}{X_B^S - X_B^1} f^{(S)} \frac{dX_B^S}{dT}$$

$$+ \frac{X_A^S \Delta H_A + X_B^S \Delta H_B^S}{X_B^S - X_B^1} f^{(1)} \frac{dX_B^1}{dT} \tag{7}$$

The quantities X_B^1 and X_B^S are read from the phase diagram

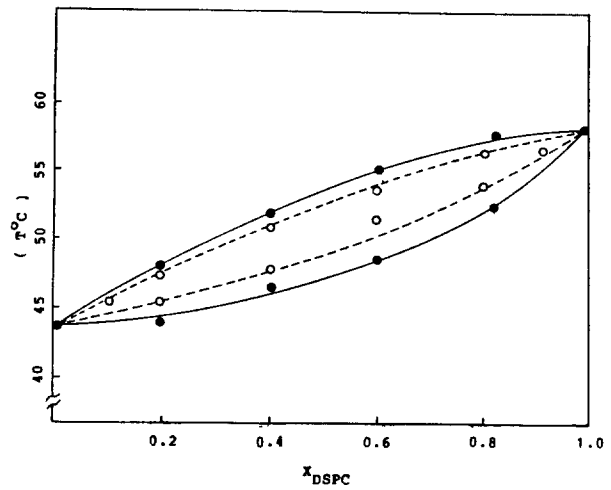

Figure 2. Ideal (----) and real (——) phase diagram constructed from initiation and completion temperatures read from observed transition curves for mixture of DPPC and DSPC.

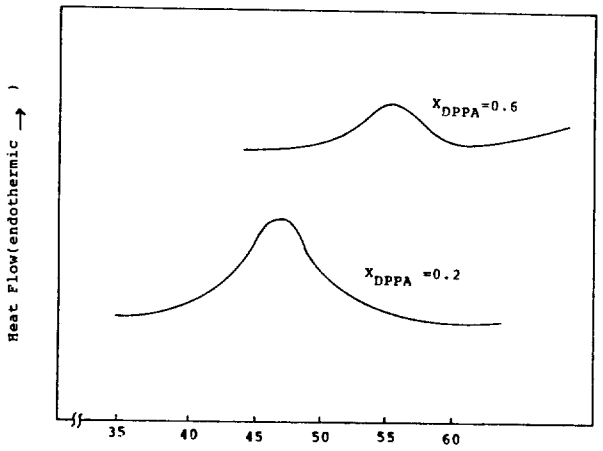

Figure 3. Calorimetric transition curves for mixture of DPPC and DPPA.

and the derivatives dX_B^l/dT and dX_B^S/dT are estimated graphically as the slopes of the liquidus and solidus curves.

Results and Discussion

The thermograms of the phospholipids mixtures in Figure 1 show broader transition temperature than those of the pure lipids. The initial and complete temperature of the mixtures for the transition were plotted in Figure 2. Ideal values were calculated with the equation (5) and included in Figure 2. The figure shows that the thermotropic properties of DPPC and DSPC mixtures do not deviate much from the ideal curves. This means that the two phospholipids are completely miscible in the liquid and solid phase. This is understandable from the fact that the two phospholipids have saturated hydrocarbon chains which differ only by two carbon atoms. The binary mixtures of the phosphatidylcholines whose saturated chains differ by only two carbon atoms show broader endothermic gel to liquid-crystalline phase transition, and such mixtures as DPPC and DSPC give ideal mixing and a single homogeneous gel phase[11,12].

Some phospholipids bear a net negative charge from a

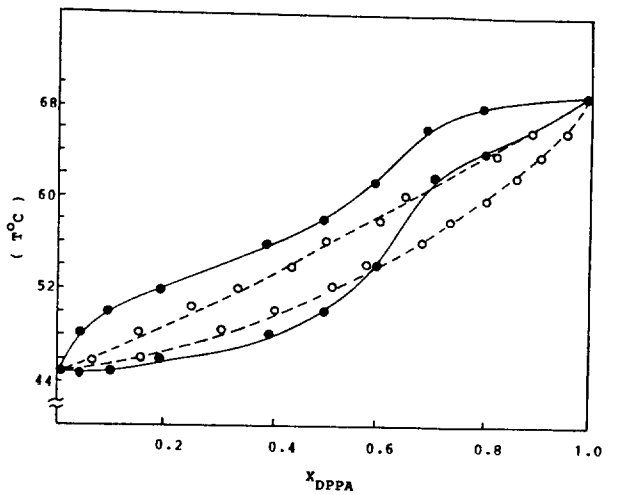

Figure 4. Ideal (----) and real (——) phase diagram constructed from initiation and completion temperatures read from observed transition curved for mixtue of DPPC and DPPA.

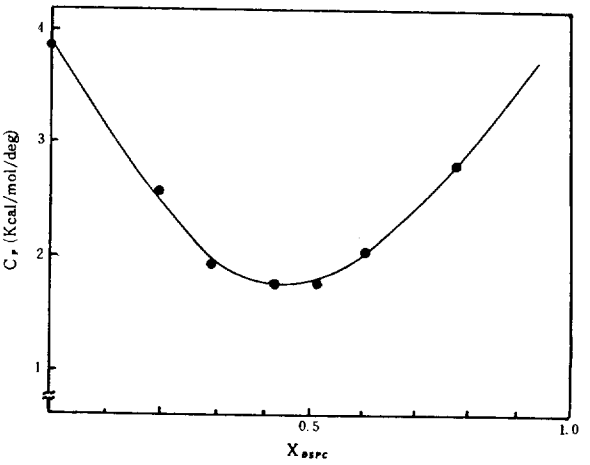

Figure 5. Plot of heat capacity *vs.* mole fraction of DPPC and DSPC at main transition temperature.

small but significant fraction of the lipid pool of most biological membranes[13-15]. One effect of ionizing DPPA may produce a more defect structure in the gel state caused by intermolecular charge repulsion. The thermograms of the phospholipid mixtures in Figure 3 show broder transition temperature than those of the pure lipids. The initial and complete temperatures of DPPC:DPPA mixtures for the transition were plotted in Figure 4. The figure shows that the thermotropic properties of DPPC and DPPA mixtures deviate much from the ideal curves. When mole percent of DPPA in DPPC:DPPA liposomes is more than 60 mol%, deviation from the ideal phase diagram became remarkable. The deviation may result from the repulsion between the head groups of acidic phospholipids. Especially, the large deviation at DPPC:DPPA liposomes containing DPPA more than 60 mol% from the ideal phase diagram may result from closely packing of phospholipids in bilayers of these compositions.

Ideal mixing has been observed with the lipids of the same headgroup and differing only slightly in alkyl chain length[4]. When head observed with the lipids of the same

headgroup and differing only slightly in alkyl chain length[4]. When head groups are different, mixing is not ideal. It is clear that the mixing properties of lipid depend on the factors that determine packing of the chains as well as the interaction between the polar groups. Mixing in the gel phase is particularly constrained because of a close packed organization.

Biological membranes are a complex mixture of phospholipid species which very with respect to both their lipid headgroups and to their associated acyl chains. As a result they do not exhibit a single well defined lipid phase transition where all of the lipid progresses from a solid to a fluid state at a well-defined temperature.

The organizational change in a bilayer that accompant a gel-to-liquid crystalline phase change is reflected in heat capacity. Heat capacity (C_p) was calculated employing equation (7). The change of heat capacity for different mole fractions of DSPC in mixed lipids at main transition temperature was shown in Figure 5. The larger C_p was, the sharper the endothermic peak became. DPPC:DSPC (60:40 mol% and 50:50 mole%) liposomes have the lower C_p than those of the others. These mixed phospholipids in gel state contain defects responsible for the formation of large angle grain boundaries of disordered region between two lipids differing in orientation or spacial arrangement. DPPC:DSPC (50:50 mol%) liposomes, of which the transition rate is the slowest of the mixed liposomes, had pronouncely reduced cooperative unit by 0.5 mM phenothiazine derivatives (not shown at this paper). Cooperative unit is the number of molecules forced to cooperate in the transition. The sharpness of a phase transition depends upon the cooperative unit.

References

1. A. Nicolussi, S. Massari and R. Colonna, *Biochemistry*, **21**, 2134 (1982).
2. M. C. Blok, L. L. M. Deenen and J. De Gier, *Biochim. Biophys.*, **433**, 1 (1976).
3. K. Jacobson and D. Papahadjoloulos, *Biochemistry*, **14**, 152 (1975).
4. M. K. Jain and R. C. Wagner, Introduction to biological membranes, John Wiley and Sons, Inc., 87 (1980).
5. Y. Barenholz, B. J. Litmann, T. E. Thompson and F. D. Carlson, *Biochemistry*, **16**, 2806 (1977).
6. D. Papahadjopoulos, *Biochim. Biophys. Acta.*, **211**, 467 (1970).
7. M. A. Singer and M. K. Jain, *Can. J. Biochem.*, **58**, 815 (1980).
8. J. M. Steim, *Methods in Enzymology*, **32**, 262 (1974).
9. D. Papahadjopoulos, *J. Colloid and Interface. Sci.*, **58**, 459 (1977).
10. J. M. Sturtevant, *Proc. Natl. Acad. Sci.*, USA., **79**, 3963 (1982).
11. S. M. Mabrey and J. M. Sturtevant, *Proc. Natl. Acad. Sci., USA.*, **73**, 3862 (1976).
12. E. N. Serrallach, G. H. de Hass and G. G. Shipley, *Biochemistry*, **23**, 713 (1984).
13. M. D. Houslay and K. K. Stanly, *Dynamics of biological membranes, John Wiley and Sons*, 39 (1982).
14. D. Hoekstra and O. C. Martin, *Biochemistry*, **21**, 6097 (1982).
15. M. Caffrey and G. W. Feigenson, *Biochemistry*, **23**, 323 (1984).

A Theoretical Investigation of FCO and FCO+

Eun-Mo Sung and Ho-Soon Lee

Department of Science Education, Chungbuk National University, Chungbuk 360-763. *Received May 18, 1990*

Ab initio calculations with MP3 and CISD method were performed for the FCO and FCO^+. The equilibrium geometry of FCO shows the reasonable agreement with experimental values. FCO^+ has a linear geometry with R_{CF}= 1.213 and R_{CO}= 1.118 Å. The quadratic force constants of FCO^+ are 23.21 md $Å^{-1}$ for CO stretch and 12.38 md $Å^{-1}$ for CF stretch. The cubic force constants and the other molecular constants are also calculated.

Introduction

The fluoroformyl radical, FCO has been the subject of many theoretical and experimental works. Because of its large reactivity the experimental works has been done mainly in low-temperature matrices. Milligan *et al.*[1] observed the three fundamental bands of FCO in both a CO and an Ar matrix. The three vibrational fundamentals appear at 1855, 1018, 616 cm^{-1}. Later, Jacox[2] extended the work and studied in more detail the vibrational and electronic spectra of FCO in Ar matrix. The three fundamental absorptions of FCO were found at 1857, 1023, 627.5 cm^{-1}. Adrian *et al.*[3,4] observed the ESR spectrum of FCO in a CO matrix and concluded that FCO is a σ radical with the large fluorine hyperfine splittings.

The FCO radical in the gas phase was detected by Jonathan *et al.*[5] using photoelectron spectroscopy. They observed the ionization potential of FCO and the deformation vibra-